NeuroImage: Clinical 28 (2020) 102379

Contents lists available at ScienceDirect

NeuroImage: Clinical

journal homepage: www.elsevier.com/locate/ynicl

Intracranial vascular flow oscillations in Alzheimer's disease from 4D flow MRI

Leonardo A. Rivera-Rivera[a], Karly A. Cody[b], David Rutkowski[c], Paul Cary[b], Laura Eisenmenger[c], Howard A. Rowley[b,c], Cynthia M. Carlsson[b,d], Sterling C. Johnson[b,d], Kevin M. Johnson[a,c,*]

[a] Department of Medical Physics, University of Wisconsin, School of Medicine and Public Health, Madison, WI, USA
[b] Alzheimer's Disease Research Center, University of Wisconsin, School of Medicine and Public Health, Madison, WI, USA
[c] Department of Radiology, University of Wisconsin, School of Medicine and Public Health, Madison, WI, USA
[d] Geriatric Research Education and Clinical Center, William S. Middleton Memorial Veterans Hospital, Madison, WI, USA

ARTICLE INFO

Keywords:
4D flow MRI
Alzheimer's disease
Low frequency oscillations
High frame rate
Vascular health
Vasomotion

ABSTRACT

Recent modeling and experimental evidence suggests clearance of soluble metabolites from the brain can be driven by low frequency flow oscillations (LFOs) through the intramural periarterial drainage (IPAD) pathway. This study investigates the use of 4D flow MRI to derive LFOs from arterial and venous measures of blood flow. 3D radial 4D flow MRI data were acquired on a 3.0 T scanner and reconstructed using a low-rank constraint to produce time resolved measurements of blood flow. Physical phantom experiments were performed to validate the time resolved 4D flow against a standard 2D phase contrast (PC) approach. To evaluate the ability of 4D flow to distinguish physiologic flow changes from noise, healthy volunteers were scanned during a breath-hold (BH) maneuver and compared against 2D PC measures. Finally, flow measures were performed in intracranial arteries and veins of 112 participants including subjects diagnosed with Alzheimer's disease (AD) clinical syndrome ($n = 23$), and healthy controls ($n = 89$) on whom apolipoprotein ε4 positivity (APOE4+) and parental history of AD dementia (FH+) was known. To assess LFOs, flow range, standard deviation, demeaned temporal flow changes, and power spectral density were quantified from the time series. Group differences were assessed using ANOVA followed by Tukey-Kramer method for pairwise comparison for adjusted means ($P < 0.05$). Significantly lower LFOs as measured from flow variation range and standard deviations were observed in the arteries of AD subjects when compared to age-matched controls ($P = 0.005$, $P = 0.011$). Results suggest altered vascular function in AD subjects. 4D flow based spontaneous LFO measures might hold potential for longitudinal studies aimed at predicting cognitive trajectories in AD and study disease mechanisms.

1. Introduction

AD is currently the 6th leading cause of death in the United States, and the only leading cause of death with rising prevalence (Dementia: Fact sheet N°362. World Health Organization (WHO), 2019). AD has no curative treatment. There is some indication that optimizing brain health including vascular health may buffer the disease and slow cognitive decline (The SPRINT MIND Investigators for the SPRINT Research Group, 2019). Associations between cerebrovascular and AD pathology (Arvanitakis et al., 2016; Sweeney et al., 2019, 2018, 2015; Toledo et al., 2013; Wåhlin and Nyberg, 2019) suggest a potential compounding influence of vascular disease on the pathologic trajectory of AD. Yet, the mechanisms relating vascular and AD disease are not clear due to lack of systematic study of AD biomarkers over time together with corresponding comprehensive vascular biomarkers.

Although the brain lacks a traditional lymphatic system for clearing waste products, it has been hypothesized that the brain possesses alternative pathways – the glymphatic system and intramural periarterial drainage (IPAD) (Hawkes et al., 2014)), both of which involve cerebral artery motion. This vascular motion includes induced vessel caliber changes from both the cardiac cycle pulsations (Weller et al., 2009) and arterial wall smooth muscle oscillations which induce low frequency flow oscillations (LFOs) (Diem et al., 2017). The relative contribution of these motions to metabolite clearance is poorly understood. Data suggests decreased vascular elasticity may cause both diminished cardiac cycle induced vessel caliber changes and diminished LFOs, thereby

* Corresponding author at: University of Wisconsin-Madison, Rm 1133, Wisconsin Institute for Medical Research, 1111 Highland Ave, Madison, WI 53705-2275, USA.
E-mail address: kmjohnson3@wisc.edu (K.M. Johnson).

https://doi.org/10.1016/j.nicl.2020.102379
Received 16 April 2020; Received in revised form 10 July 2020; Accepted 7 August 2020
Available online 12 August 2020

slowing clearance of metabolites (Di Marco et al., 2015; Plog and Nedergaard, 2018).

Magnetic resonance imaging (MRI) is a non-invasive technology that can be used longitudinally, and offers a vast array of techniques to probe key components of vascular involvement in AD; however, past and ongoing studies in AD have largely inferred vascular disease based on the quantification of white matter hyperintensities (WMH) seen on T2 FLAIR MRI (Wardlaw et al., 2013) and from reduced cerebral blood flow (CBF). Such studies have found correlations with AD and hypoperfusion (Clark et al., 2017), WMH burden (Birdsill et al., 2014), and decreased intracranial macrovascular blood flow (Berman et al., 2017, 2015; Rivera-Rivera et al., 2017, 2016); though, hypoperfusion and WMH's are not specific to cerebral vascular pathology and occur in other diseases and in normal aging (Alber et al., 2019). More specific measures are needed to elicit the mechanisms of involvement between cerebrovascular disease (CVD) and AD pathologies. LFOs can provide measures of active vascular distention, a potential driving force of metabolic clearance in the brain. Further, LFOs can be used to probe physiologic, autoregulatory flow changes. Recent studies using near-infrared spectroscopy (NIRS) have shown alterations of LFOs in cognitive decline and cerebrovascular disease (Andersen et al., 2018; Quaresima and Ferrari, 2016; Zeller et al., 2019). Further, LFOs from fMRI BOLD techniques (Obrig et al., 2000; Tong et al., 2019a, Tong et al., 2012) have shown large interference with resting state connectivity mapping.

Intracranial four-dimensional (4D) flow MRI has the potential to measure LFOs overcoming fundamental limitations of other techniques such as the neural signal contamination of fMRI BOLD or depth sensitivity of NIRS. 4D flow MRI has the ability to probe vessels directly; however, this has not been possible in past studies due to relatively slow data acquisition of 4D flow MRI protocols. Time-resolved, three-dimensional, phase contrast velocimetry measurements, well known as 4D flow MRI, can be accelerated using 3D radial sampling to enable high spatial resolution and field-of-view needed to provide whole brain coverage and the quantification of blood velocities in the brain's feeding arteries and draining veins (Johnson et al., 2008; Rivera-Rivera et al., 2016; Vikner et al., 2019). 4D flow MRI has also been used to probe transcranial vascular stiffness in AD subjects by means of pulse wave velocity (PWV), the gold standard non-invasive biomarker of arterial stiffness (Laurent et al., 2006; Rivera-Rivera et al., 2020). Higher PWV was measured in AD dementia clinical syndrome when compared to age-matched controls. In that study, 4D flow was combined with a constrained reconstruction approach in order to increase the temporal resolution of the reconstructed cardiac phase; however, in order to measure LFOs, instead of reconstructing the high frequency cardiac phases (e.g. the cardiac cycle), a time resolved reconstruction that allows characterization of lower frequencies (e.g. < 0.2 Hz) is desirable.

Here we used a constrained reconstruction based on low-rank representation of 4D flow data to investigate the feasibility of LFO measures from intracranial arteries and veins. The high frame rate time reconstruction allowed tracking of brain vascular physiological changes such as autoregulation and respiration effects. Flow rates from the 4D flow reconstruction were validated against standard 2D methods in phantom and volunteer experiments. Subsequently, LFOs were measured in the intracranial arteries and veins of AD subjects, older cognitively unimpaired controls, and healthy late middle-aged subjects with apolipoprotein ε4 positivity (APOE4+) and parental history of AD dementia (FH+). It was hypothesized LFOs would be quantifiable and distinguishable from noise, and diminished in AD subjects.

2. Materials and methods

2.1. Phantom validation experiments

A physical model was used to validate flow measurements from the constrained 4D flow MRI reconstruction against a standard 2D PC MRI reconstruction approach. The phantom model consisted of a straight, transparent poly-vinyl chloride (PVC) perfusion tube (inner diameter = 6 mm, outer diameter = 9 mm) connected to a positive displacement pulsatile pump with a hemodynamic conditioning head (BDC PD-1100, BDC Laboratories, Wheat Ridge, CO). The pump generated a sinusoidal waveform at 60 beats per minute (bpm). A mixture of 60% glycerol and 40% distilled water was used for a viscosity similar to that of blood (3.5cP) (Summers et al., 2005). Three experiments were performed; during these experiments, flow rate was varied cyclically from a reference flow rate of 17 mL/s along the inner diameter of the straight tube as determined from probe measurements (Transonic PXL Flowsensor) performed before and after each experiment. During the first experiment, flow rate was varied every minute throughout the length of the scan by ± 20%. For the second and third experiments, flow rate was varied by ± 10% and ± 5% respectively. In a fourth experiment, flow rate was varied by ± 20%; however, MRI acquisitions were acquired will all encodings first-order gradient moment nulled (e.g. flow compensated) in order to estimate measurement variances while maintaining similar levels of inflow-based enhancement. Additional details of these experiments are described below in section 2.4.1 Imaging protocol.

2.2. Volunteers breath-hold experiments

To evaluate the ability of 4D flow to distinguish physiologic changes from noise in vivo, five healthy volunteers (mean age = 28 ± 4y, 2F) were scanned with a protocol which included a breath hold (BH) maneuver during 4D flow and 2D PC MRI acquisitions. The volunteers were trained to perform a single ~20 s BH after a long inspiration. Volunteers were signaled from the control room and the BH was performed halfway through the scan.

2.3. Subjects and clinical classification

Study participants were recruited from the Wisconsin Alzheimer's Disease Research Center (WADRC) and Wisconsin Registry for Alzheimer's Prevention (WRAP) (Johnson et al., 2018). Data from 112 subjects (mean age = 66 ± 10 years) were analyzed (demographic data, Table 1). Study groups included cognitively healthy older adults, AD dementia clinical syndrome subjects, and cognitively healthy late middle-aged adults. The late middle-aged (age 45 to 65 years) subjects were classified into two groups, APOE4-, FH-, and APOE4+, FH+, due to absence or presence of both APOE4 allele and parental family history of AD dementia. Participants were diagnostically characterized in the Wisconsin ADRC's multidisciplinary consensus conferences using applicable clinical, laboratory, and imaging criteria (Albert et al., 2011; Jack et al., 2018; McKhann et al., 1984, 2011; Sperling et al., 2011). The University of Wisconsin Institutional Review Board approved all study procedures and protocols following the policies and guidance established by the campus Human Research Protection Program (HRPP). All study procedures were performed according to the Declaration of Helsinki, including obtaining written informed consent from each participant. Subjects were excluded if given a consensus diagnosis of a non-Alzheimer's variant of dementia (e.g. Frontotemporal Dementia, Lewy Body Dementia, or Vascular Dementia). In addition, exclusion criteria overseen by the clinical supervising physician (C.M.C) included significant medical conditions such as major systemic illness or cancer. MRI scans were reviewed by a neuroradiologist (H.A.R.) for incidental findings.

2.4. Imaging protocol

2.4.1. Phantom validation experiments

Time-resolved 2D and 3D PC MRI data were acquired on a 3.0 T system (MR750, GE Healthcare) using radial acquisitions (Johnson et al., 2008) and a 32-channel head coil (Nova Medical, Wilmington,

Table 1
Demographic information.

	Total (n = 112)	AD (n = 23)	Older Cognitively healthy (n = 36)	Middle-aged APOE4 +, FH + (n = 23)	Middle-aged APOE4-, FH- (n = 30)
Age (years)	66 ± 10	72 ± 10	73 ± 7	59 ± 3	57 ± 5
Female (n, %)	76, (68%)	16, (70%)	21, (58%)	17, (74%)	22, (73%)
Parental dementia history positive (n, %)	36, (32%)	11, (48%)	2, (6%)	23, (100%)	0, (0%)
APOE ε4 carrier (n, %)*	33, (29%)	9, (39%)	1, (3%)	23, (100%)	0, (0%)
SBP (mmHg)	127 ± 18	132 ± 20	132 ± 23	123 ± 11	122 ± 14
DBP (mmHg)	77 ± 8	75 ± 7	77 ± 10	76 ± 7	79 ± 7
HR (bpm)	60 ± 9	61 ± 10	62 ± 9	61 ± 7	59 ± 10
CHS scores	2.3 ± 1.7	3.5 ± 2.3	2.7 ± 1.6	1.4 ± 0.6	1.6 ± 1.0

Abbreviations: AD, Alzheimer's disease; APOE, apolipoprotein E; FH, family history; DBP, diastolic blood pressure; HR, heart rate; SBP, systolic blood pressure; CHS, Cardiovascular Health Study. Seven subjects not genotyped (five AD, two middle-age APOE4-, FH-); carrier refers to presence of at least one APOE ε4 allele.

MA). For 2D PC MRI, data were acquired with the following imaging parameters: field of view = 22 × 22cm^2, slice thickness = 10 mm, TR/TE = 8.6/3.9 ms, and number of projections ~21,000. For 3D, parameters were: acquisition imaging volume = 22 × 22 × 10 cm^3, TR/TE = 8.6/2.5 ms, number of projections ~10,500. For both 2D and 3D acquisitions, scan time was ~ 6 min, acquired spatial resolution = 0.7 mm (in plane for 2D, isotropic for 3D), flip angle = 8°, bandwidth = 250 kHz, and V_{enc} = 120 cm/s. For 2D, a single slice orthogonal to the tube length was acquired.

2.4.2. Volunteer breath-hold experiments

Using the same scanner and coil as for the phantom experiments, time-resolved radial 2D and 3D PC MRI were acquired with the following imaging parameters: for the 2D acquisition, field of view = 22 × 22cm^2, slice thickness = 5 mm, TR/TR = 8.6/4.1 ms, number of projection ~22 000, V_{enc} = 80 cm/s; for the 3D acquisition, imaging volume = 22 × 22 × 10cm^3, TR/TE = 8.6/2.6 ms, number of projections ~11 000, and V_{enc} = 100 cm/s. For both 2D and 3D scans, acquired spatial resolution = 0.7 mm (in plane for 2D, isotropic for 3D), flip angle = 8°, and bandwidth = 250 kHz. The 2D single slice scan was acquired axial to the posterior inferior portion of the superior sagittal sinus (SSS). Compared to phantom validation experiments, a smaller slice thickness (e.g. 5 mm) was prescribe in volunteer experiments to improve plane alignment with respect to vessel curvature. The 4D flow scan was volumetric, thus included both arteries and veins. A slightly higher V_{enc} was prescribe for the 4D flow scan to avoid potential arterial velocity aliasing during the physiological challenge.

2.4.3. MR imaging in study subjects

Volumetric, time-resolved 3D PC MRI data were acquired using the same scanner and head coil as for the phantom and volunteer experiments. Data were acquired using the same radial sequence with the following imaging parameters: V_{enc} = 80 cm/s, imaging volume = 22 × 22 × 10 cm^3, TR/TE = 7.4/2.7 ms, scan time ~7.2 min, acquired spatial resolution = 0.7 mm isotropic, flip angle = 8°, bandwidth = 250 kHz, number of projections ~11,000. Cardiac triggers were collected for each subject from a photoplethysmogram on a pulse oximeter worn on the subject's finger during the exam. T1-weighted data were also acquired using a 3D inversion-recovery prepared fast spoiled gradient-echo sequence using the following parameters: inversion time (TI) = 450 ms, TR = 6.0 ms, TE = 2.2 ms, flip angle = 12°, imaging volume = 25.6x × 25.6 × 13.0 cm^3, in-plane resolution 1 mm, slice thickness = 1.2 mm. Cushions inside the head coil were used to reduce head movement during scanning. CSF and intracranial volume (ICV) were segmented using SPM12 (www.fil.ion.ucl.ac.uk/spm) as described previously (Allison et al., 2019). In addition, 3D T2-weighted fluid attenuated inversion recovery (FLAIR) images were acquired using TI = 1868 ms, TR = 6000 ms, TE = 123 ms, flip angle = 90°, FOV = 25.6 × 25.6 cm^2, slice thickness = 2.0 mm and spatial resolution = 1 × 1 × 2mm^3. Subsequently, T2FLAIR images were evaluated by two neuroradiologists (H.A.R., L. E.) blinded to clinical variables. From T2FLAIR images white matter hyperintensity (WMH) burden was quantified using the Cardiovascular Health Study (CHS) scale, where a "0" represents no evidence of WMH lesion and a "9" reflects involvement of all white matter (Manolio et al., 1994; Moghekar et al., 2012).

2.5. Image reconstruction and post processing

2.5.1. High frame rate time-resolved 4D flow reconstruction

Images were retrospectively reconstructed using GPU accelerated (SigPy) (Ong and Lustig, n.d.) iterative SENSE (Pruessmann et al., 1999) with JSENSE (Ying and Sheng, 2007) sensitivity maps and a local-low rank temporal constraint (Jimenez et al., 2018; Trzasko and Manduca, 2011). The low rank temporal constraint was enforced using a nuclear norm minimization. Reconstructions were performed with block shifting of a 16x16x16 block and an empirically tuned regularization parameter (λ = 0.0001). Reconstruction time was approximately 13 h.

Velocity data time series were reconstructed into 100 frames. The temporal constraint reconstruction was used to lessen noise and artifacts inherent with high frame rate binning of undersampled data. In addition, spatial resolution was traded off for higher temporal binning and images were reconstructed to an isotropic spatial resolution of 1.38 mm.

2.5.2. Standard 2D PC and 4D flow MRI reconstructions

Iterative SENSE was also used to reconstruct 2D PC MRI data from both phantom and volunteer experiments. No temporal or spatial constraint was necessary since data were not substantially undersampled. Similar to 4D flow, 2D PC images were reconstructed to 100 time frames.

4D flow MRI data were also reconstructed with gating to the cardiac cycle. This was done to compare high frequency cardiac variations with LFO measures derived from time reconstructed images. As described in previous work (Rivera-Rivera et al., 2017), these images were reconstructed using SENSE, spatial resolution was 0.7 mm isotropic, and 20 cardiac phases that were retrospectively generated (temporal resolution ~50 ms) using vendor supplied detected gate positions from a pulse oximeter.

2.5.3. Velocity and flow processing

The time series of the magnitude data were inspected for motion artifacts (L.A.R.R.) and subjects with evidence of moderate motion (> 1 voxel) were excluded from the analysis. Subject flow measurements were derived in the internal carotid artery (ICA) bilaterally and in the posterior inferior portion of the superior sagittal sinus (SSS). Measurements were performed in MATLAB on the time-resolved data (Schrauben et al., 2015). Cross-sectional area and vessel lumen were automatically outlined from time-average 4D flow and 2D PC datasets.

Flow rates were estimated from the product of cross-sectional areas and velocities. Background phase correction of velocities were performed by fitting polynomials through the phase of static tissue. The vasculature was segmented using a centerline process with local cut-planes automatically placed in every centerline point perpendicular to the axial direction of the vessel. Time-averaged regions of interest (ROIs) were automatically contoured using a k-means clustering approach under the assumption that any cross section will contain a low-signal background and a vessel region. Besides flow, max velocity was also measured in the ICA and SSS. Max velocity was the maximum velocity enclosed in the vessel mask. This velocity measurement closely corresponds to the max velocity measure that might be derived from ultrasound, and it is also less sensitive to the vessel mask. Phantom data were also processed in MATLAB, and flow measurements on 4D datasets were performed in the same location of the 2D scan slice.

2.5.4. LFO analysis

Velocity and flow range (max – min) were estimated for both time-resolved reconstructed data (flow range during scan length) and cardiac cycle reconstructed data (flow range during the cardiac cycle (e.g. high frequency changes)). Demeaned flow changes were also quantified from the time series. Standard deviations (σ) of the flow profiles throughout the scan length were also estimated as a marker for LFOs. Further, standard deviations were normalized to total brain volume (ICV-CSF). Average blood flow rates were also quantified. Fourier transforms were performed on the flow and velocity time series and the power spectral density (PSD) of flow and velocity oscillations were calculated between 0.002 and 0.116 Hz. To compare hemodynamic response between groups, mean PSD were estimated. Measurements of transcranial pulse wave velocity (PWV) were included as described previously (Rivera-Rivera et al., 2020) in order to compare with LFO analysis.

2.5.5. Statistical analysis

Velocity and flow metrics were compared between groups. Furthermore, heart-rates, systolic, and diastolic blood pressure differences were evaluated between AD and age-matched controls as well as between late middle-aged APOE4+, FH+ and APOE4-, FH- subjects. The differences in these measurements were assessed using ANOVA followed by post hoc analysis using the Tukey-Kramer method. Statistical analysis was performed in MATLAB. $P < 0.05$ was set as the threshold for statistical significance.

3. Results

3.1. Phantom experiments

Temporal resolution in phantom experiments was 3.6 s in both 4D and 2D scans. Findings from the phantom experiments are summarized in Fig. 1. Good agreement between 2D and 4D flow measures was found with larger standard deviation in 4D measurements. The average temporal mean of 2D and 4D flow measurements were: 17 mL/s, 17 mL/s for 20% variation (a), 17 mL/s, 17 mL/s for 10% variation (b), and 17 mL/s, 17 mL/s for 5% variation (c). The standard deviation, min and max of 2D and 4D flow measurements were: 2.6 [13, 21] mL/s, 2.6 [12, 21] mL/s for 20% variation (a), 1.3 [15, 19] mL/s, 1.3 [15, 19] mL/s for 10% variation (b), and 0.65 [16, 19] mL/s, 0.71 [15, 19] mL/s for 5% variation (c). The standard deviation of the flow compensated acquisition were 0.04 mL/s for 2D and 0.15 mL/s for 4D (histogram of the flow rates (d)). Inflow and intravoxel dephasing effects on these data were observed in the magnitude signal time series (supplementary Fig. 1).

3.2. Volunteer breath-hold experiments

Volunteer BH data are showed in Fig. 2. Scan time was 6.3 min for a temporal resolution of 3.8 s in both 4D and 2D scans. Volunteer breathing patterns were recorded during the scans using respiratory bellows and these records are available in supplementary Fig. 2. The temporal location of the 20 s BH is marked in Fig. 2 as visually determined from respiratory bellow data. Overall, good agreement is observed between 2D and 4D flow measurements in the SSS; however, a larger response to the BH was measured using the 2D technique in most volunteers. 2D measurements also showed larger standard deviation throughout the time series. A quantitative summary is available in Table 2.

3.3. Study subjects

For the study subjects, temporal resolution of 4D data was 4.3 s (scan time ~7.2 min). No significant differences ($P > 0.05$) between blood pressure (systolic and diastolic) and heart rate were found between AD, age-matched controls, or between middle-aged APOE4+, FH+ and middle-aged APOE4-, FH- groups. WMH burden CHS scores were largest in the AD group (CHS = 3.5 ± 2.3) (Table 1), but differences were not significant when compared to age-matched controls (CHS = 2.7 ± 1.6). No significant differences in CHS scores were found between middle-aged APOE4-, FH- (CHS = 1.4 ± 0.6) and middle-aged APOE4+, FH+ (CHS = 1.6 ± 1.0). Time-resolved 4D flow magnitude images were inspected for bulk motion. Data from subjects described in Table 1 did not show evidence of major motion (> 1 voxel) during the 7.2 min scan; however, of the 126 subjects imaged, 14 subjects had identifiable motion and were excluded. An example dataset of bulk motion is included as supplementary Fig. 3 (.GIF animation).

Demeaned ICA flow LFOs for every subject are displayed as intensity plots in Fig. 3. LFOs in the ICA were noticeably smaller in the AD group (a). LFOs were largest in APOE4+, FH+ (d), followed by APOE4-, FH- (c) and age-matched controls (b). Flow range from low frequency data (a) (time-resolved recon) and high frequency cardiac data (b) (cardiac-resolved recon) are summarized in Fig. 4. A significantly reduced low frequency range of flow in the ICA was measured in AD subjects when compared with age-matched controls and the other groups (AD vs age-matched control ICA flow range $P = 0.005$) (P-values from group comparisons are in Table 3). A similar trend was observed in the high frequency cardiac range measurements, where AD group flow range was lower, although not significantly.

Standard deviations of ICA blood flow (Fig. 5(a)) during the time-resolved acquisition were also significantly lower in AD when compared to others (AD vs age-matched control flow standard deviation $P = 0.011$, other group comparisons p-values are summarized in Table 3). After normalizing ICA standard deviation to brain volume, significant differences between AD and age-matched controls persisted (Fig. 5(b)) (AD vs age-matched control normalized flow standard deviation $P = 0.040$). Lower average blood flow rates (Fig. 6) in both the ICA and SSS were measured in the AD group followed by age-matched control, APOE4-, FH-, and APOE4+, FH+ groups.

Group flow PSDs are summarized in Fig. 7. Lower LFOs were measured in AD subjects PSD (Fig. 7(a, c)) in arteries and veins when compared to age-matched controls and the other groups. Largest flow LFOs were measured in the PSD of the APOE4+, FH+ subjects (Fig. 7(b, d)).

Results for max velocity range, standard deviation, and PSDs are shown in supplementary Figs. 4–6 and supplementary Table 1. Max velocity group differences were similar to flow group differences. Linear regression age analysis of max velocity low frequency range and standard deviation (supplementary Fig. 7) showed weakly linear correlation coefficients in both groups, with late middle-aged APOE4+, FH+ adults demonstrating higher average values for both parameters and a positive slope, compared to a negative slope in late middle-aged APOE4-, FH- adults. Transcranial PWV measures along the ICA are summarized in supplementary Fig. 8. Transcranial PWV was significantly higher in AD subjects (vs age-matched controls $P < 0.001$,

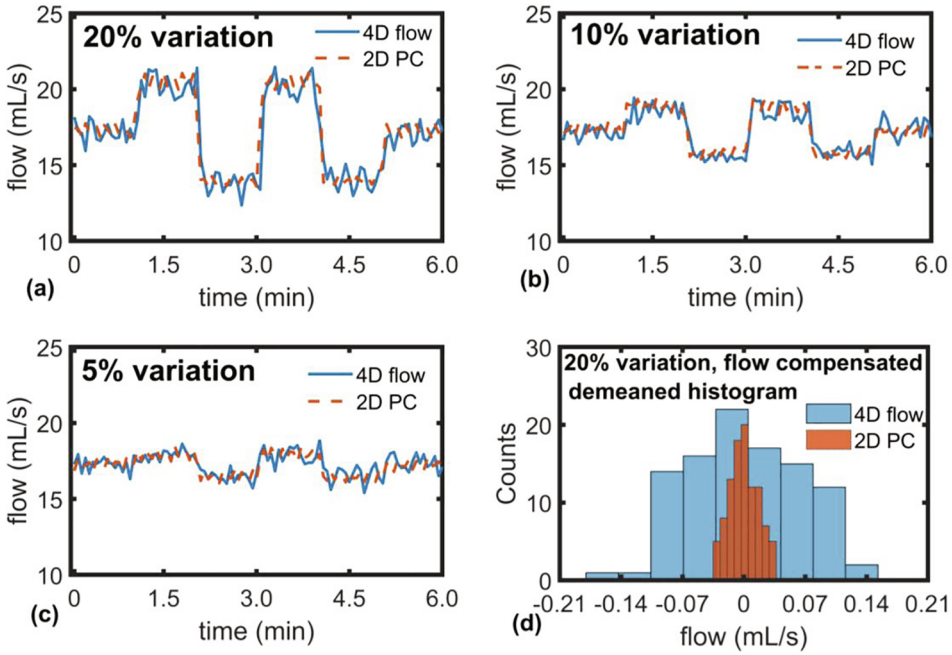

Fig. 1. Line plots (a, b, c) and a histogram (d) showing flow results from phantom experiments where 4D and 2D scans were acquired (scan time = 6 min, temporal resolution = 3.6 s) axially to a straight poly-vinyl chloride (PVC) tube that was connected to a pulsatile pump that generated a sinusoidal flow waveform at a rate of 60 beats per minute (bpm). Pump flow rates were varied each minute throughout the scan by factors of: ± 20% (a), ± 10% (b), and ± 5% (c). In a fourth experiment, flow was varied by ± 20% (d); however, MRI acquisitions were first-order gradient moment nulled (e.g. flow compensated) to estimate measurement variances. The histogram of the flow compensated acquisitions showed larger variance in 4D measures compared to 2D.

vs APOE4-, FH- $P < 0.001$, vs APOE4+, FH+ $P < 0.001$), while age-matched controls and APOE4+, FH+ has similar PWV ($P = 0.923$). APOE4-, FH- had the lowest PWV in this cohort (vs APOE4+, FH+ $P = 0.002$, vs age-matched control $P = 0.005$). Regression analysis of transcranial PWV (supplementary Fig. 9) showed a weak correlation with blood flow range ($R^2 = 0.058$) (a) and blood flow standard deviation ($R^2 = 0.051$) (b).

4. Discussion

This study evaluated intracranial arterial and venous LFOs in AD subjects, age-matched controls, late middle-aged healthy subjects with

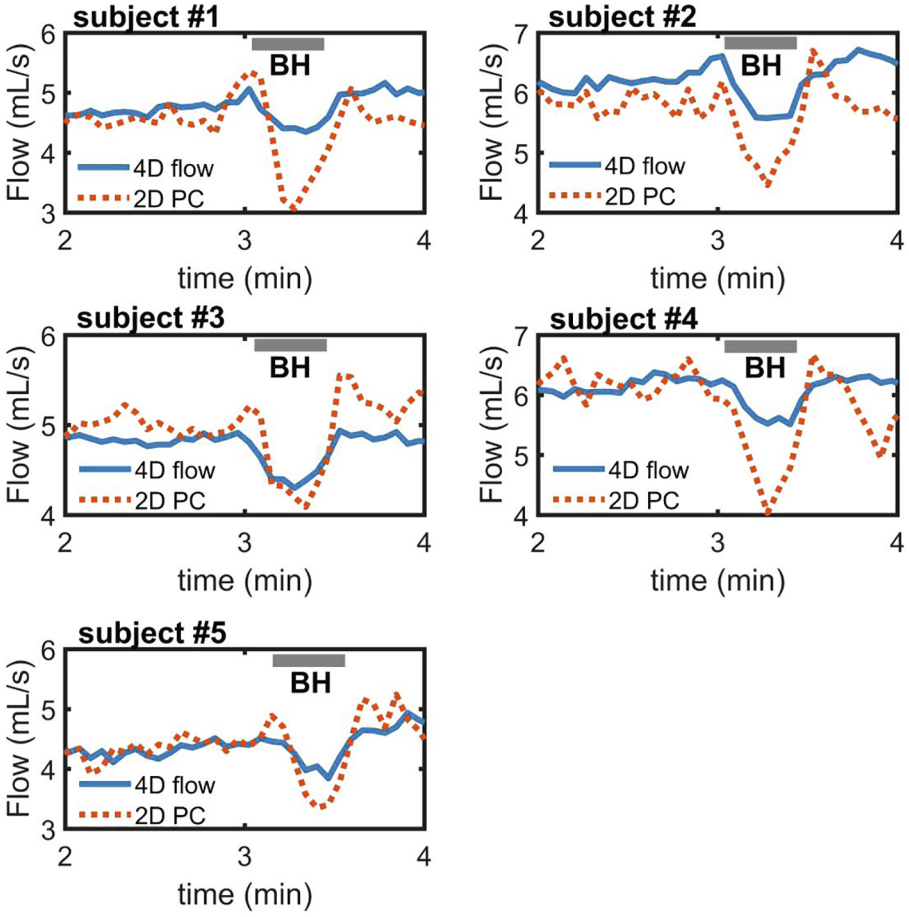

Fig. 2. Line plots showing 4D and 2D flow data measured in the superior sagittal sinus (SSS) in five healthy volunteers during a 20 s breath hold (BH). Both scans were 6.3 min long (temporal resolution = 3.8 s). Subjects were instructed to hold their breath after a long inspiration; after 20 s the subjects were instructed to end the BH. Rectangle bars indicate when BHs occurred. Both 4D and 2D scans data demonstrated a physiological response to the BH; however, a larger flow response and standard deviation was observed in 2D measurements. Respiratory bellow data is available in supplementary Fig. 2.

Table 2
Volunteer breath hold (BH) data.

	temporal average (mL/s)		standard deviation [min, max] (mL/s)	
	2D scan	4D scan	2D scan	4D scan
subject 1	4.5	4.8	0.34 [3.1, 5.4]	0.17 [4.3, 5.1]
subject 2	6.2	6.2	0.43 [4.6, 7.0]	0.27 [5.4, 7.0]
subject 3	4.8	4.8	0.31 [4.1, 5.5]	0.10 [4.5, 5.1]
subject 4	5.9	6.2	0.47 [4.1, 6.8]	0.18 [5.6, 6.5]
subject 5	4.2	4.5	0.30 [3.3, 5.1]	0.18 [3.9, 4.8]

APOE4 + , FH + and APOE4- and FH- using time reconstructed 4D flow MRI. High frame rate, ungated 4D flow imaging was achieved using a local low-rank constrained approach. First, the high frame rate 4D reconstruction was validated against a standard 2D PC method in a phantom model, in which, good agreement between techniques was observed. Second, 4D PC was validated in vivo in healthy volunteers in a scan that included a 20 s BH in order to demonstrate the capacity to distinguish physiological changes from noise. Good agreement was also found in in vivo experiments between 4D and 2D methods, and BH induced flow variations were characterized from the time series. Using 4D flow, diminished LFOs were measured in AD subjects compared to age-matched controls, APOE4 + , FH + , and APOE4-, FH-. These results suggest decreased vasomotion in the cerebrovasculature of clinically diagnosed AD subjects. In addition, the largest LFOs were measured in late middle-aged adults with APOE4 + and FH + . Notably, this is the first study that uses high frame rate, time reconstructed, 4D flow MRI to quantify intracranial LFOs in AD subjects.

LFO findings in this work agree well with other studies that used NIRS in mild cognitively impaired (MCI), older healthy subjects, and younger healthy subjects. In prior work (Zeller et al., 2019), lower LFOs were observed in MCI when compared to healthy elderly subjects. Further, in our study, the late middle-aged APOE4 + , FH + group (higher AD risk) showed higher intensity LFOs in the ICA and SSS when compared with the late middle-aged APOE4-, FH- group (lower AD risk), a result which might indicate to potential compensatory processes. The origin of observed LFOs has not been conclusively determined; LFOs studies using NIRS or fMRI have related LFOs signal to autoregulation mechanisms, partial pressure of carbon dioxide (paCO2), respiratory modulated fluctuations, blood pressure changes, and low frequency neuronal waves, among other origins (Tong et al., 2019b). LFOs variation can be induced during physiological challenges such as hypercapnia (Obrig et al., 2000), showing sensitivity in flow/vascular distension. Multimodal NIRS/fMRI approaches have also demonstrated that a major component of LFOs comes from the propagation of endogenous global blood flow and oxygenation fluctuations through the cerebral vasculature, rather than from local variations in neuronal activation or localized cerebral blood flow changes (Tong and Frederick, 2010). LFOs can also vary with tissue types (gray vs white matter), linking LFOs to biomechanical parenchymal properties (Tong et al., 2016). Recently, a BOLD-based resting-state fMRI study found higher aortic PWV was associated with lower variance in resting-state BOLD signal and lower BOLD-based resting-state functional connectivity (Hussein et al., 2020). These results indicate a substantial effect of age-related rs-fMRI differences driven by vascular changes rather than by brain function. Those findings are in line with measures of higher transcranial PWV (Rivera-Rivera et al., 2020) and lower LFOs in clinically diagnosed AD patients. Therefore, there is increased potential of using LFOs to study impaired autoregulation, vasomotion, alterations in cerebrovascular health, and coupling between vascular response and brain tissue dynamics. An advantage of 4D flow MRI based LFOs is that signal is measured directly from the vasculature, whereas both NIRS and fMRI LFOs come from tissue measurements that require signal modeling to disentangle neuronal signal contributions; however, 4D flow LFO measures are restricted to large caliber vessels.

Extracellular amyloid plaque deposits in the brain, a biomarker for AD (Jack et al., 2018), have been linked to impaired mechanisms for drainage of solutes and waste products from the brain (Jessen et al., 2015). Amyloid plaque accumulation can also happen in cerebral arteries leading to cerebral amyloid angiopathy (CAA), a condition that increases the risk for stroke. A critical barrier to understanding AD pathogenesis and concomitant vascular pathology is the lack of precise methods to measure vascular degeneration and its interaction with tissue damage, Aβ and tau pathology, and neurological decline. Recent

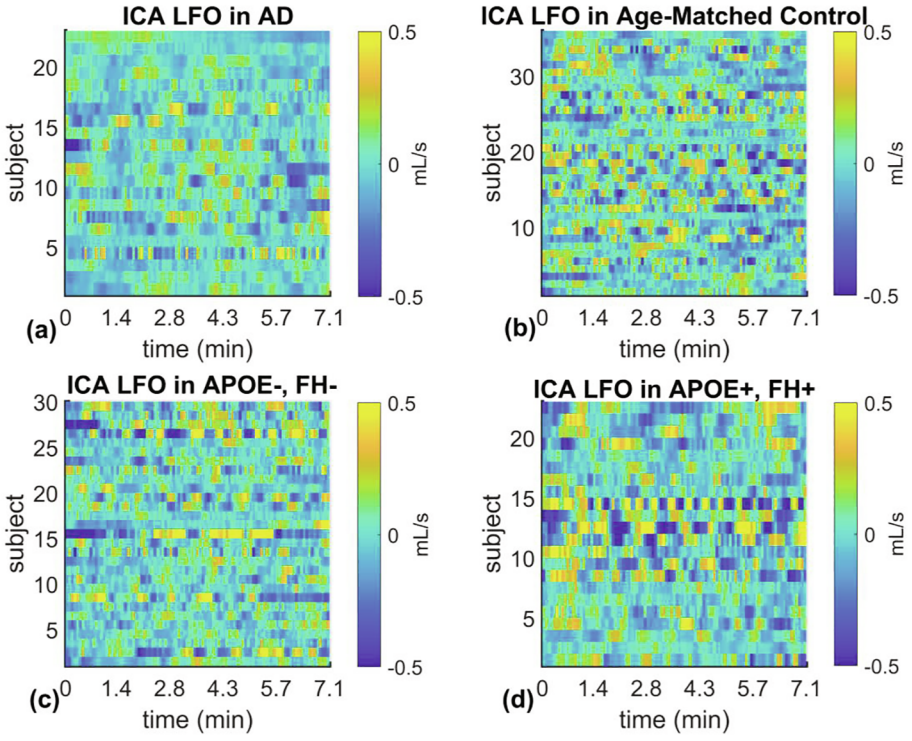

Fig. 3. Intensity plots showing low frequency oscillations (LFOs) measured as demeaned flow signal throughout 7.2 min of 4D flow scanning in the internal carotid artery (ICA) for every subject including Alzheimer's' disease (AD) subjects (n = 23) (a), age-matched control subjects (n = 36) (b), late middle-aged APOE4-, FH- (n = 30) (c), and late middle-aged APOE4 + , FH + subjects (n = 23) (d). One-hundred time frames were reconstructed for a temporal resolution of 4.3 s. The AD subjects showed lower LFOs throughout the length of the scan in the ICA when compared to other groups.

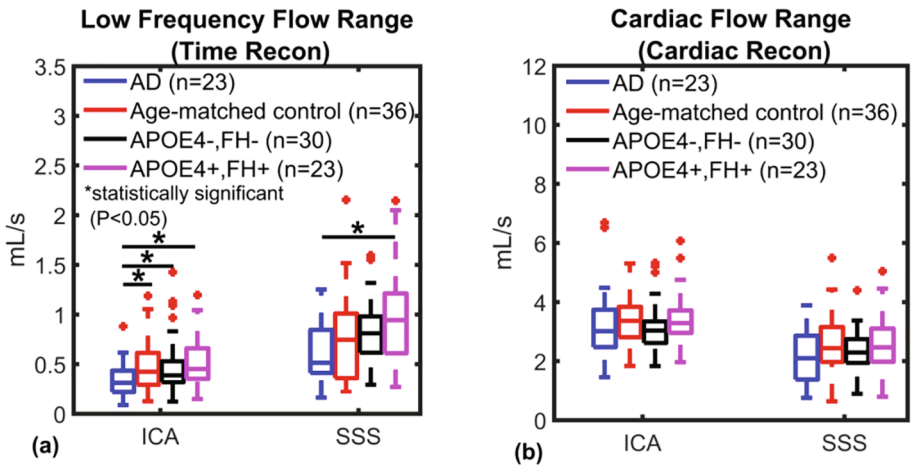

Fig. 4. Box plots showing low frequency flow range (a) (from real time reconstruction) and cardiac flow range (b) (from cardiac reconstruction) in Alzheimer's' disease (AD) subjects (n = 23), age-matched control subjects (n = 36), late middle-aged APOE4-, FH- subjects (n = 30), and late middle-aged APOE4 +, FH + subjects (n = 23). Low frequency range in AD was significantly lower when compared to other groups; however, cardiac range differences in AD were not significantly different.

models suggest clearance of soluble metabolites from the brain can be driven by LFOs of vascular smooth muscle cells through the IPAD pathway (Carare et al., 2020; Diem et al., 2017). Moreover, experimental studies in mice using two-photon microscopy have observed spontaneous LFOs in mice arterioles, and the results supported LFO driven vasomotion paravascular clearance of solutes from the brain (van Veluw et al., 2020). The researchers correlated loss of vascular smooth muscle cells and reduced vasomotion with impaired clearance of amyloid in CAA models. Their results also showed that drainage of solutes occurs along the arteries but not along the veins. This might help explain why in this study most significant LFO differences between AD and other groups were measured in arteries but not in veins. Results from that experiment also suggest that a temporal resolution of 1 s might be optimal to detect LFOs; however, this was done in mice and human LFOs range can be different due to multiple factors such as differences in blood vessel size, heart rate, blood pressure, cardiac output, etc. In another recent two-photon microscopy mice study, arteriolar endothelial cells were found to be major contributors to neurovascular coupling and vasodilation by relaying signals from the central nervous system to smooth muscle cells (Chow et al., 2020). These findings in animal models should motivate further vascular research that might in turn lead to therapeutic options aimed at improving vascular activity for removal of soluble Aβ from the brain and to preserve endothelial and smooth muscle cells for prevention of CAA and other pathology. These experiments were performed in animal models using a two-photon microscopy setup; however, LFOs from noninvasive 4D flow MRI can be used to probe the intracranial vasculature directly in human models.

Both the glymphatic system and IPAD has been suggested to be major pathways of brain clearance responsible of removing toxic metabolites including amyloid-β (Aldea et al., 2019; Iliff et al., 2012). For a long time cardiac pulsations have been hypothesized to drive glympathic flow and recent evidence in animal models suggests CSF flow through perivascular spaces, important for clearance of waste products, is in fact driven by cardiac pulsation and reduced in hypertension models (Mestre et al., 2018). On the other hand, researchers have suggested cardiac pulsations are of the wrong amplitude and frequency to drive metabolites out of the brain through the IPAD pathway. As mention before, results from animal models suggests LFOs can in fact generate vasomotion that drives perivascular clearance of solutes from the brain and that paravascular clearance is impaired in the context of cerebral amyloid angiopathy (Diem et al., 2017; van Veluw et al., 2020). Importantly, dynamic vascular information cannot be assessed from static measures of cerebral blood flow and perfusion. In this study, both cardiac flow pulsations range (~1Hz or 1 bps) and LFOs (~0.1 Hz) were investigated using 4D flow MRI by reconstructing images gated to the cardiac cycle and time respectively. Moreover, both cardiac pulsations and LFOs were lower in clinically diagnosed AD subjects; however, only LFOs were statistically different between AD and controls. Furthermore, transcranial PWV (supplementary Fig. 8), a marker of arterial stiffness derived from the high frequency cardiac flow waveforms (e.g. cardiac pulsations) was significantly higher in AD than in controls. These findings suggest increased arterial stiffness and decrease vasomotion, meaning both cardiac pulsations and LFOs changes can be correlated with an AD clinical diagnosis. Ultimately, we need studies that investigate the interactions between cardiac pulsations and LFOs with AD pathology (e.g. amyloid and tau protein) to elucidate the type of relationship between cerebrovascular health and AD.

The pulse produced by the heart travels from arteries to tissue and

Table 3
P-values from group flow comparisons.

	AD vs Control	AD vs APOE4-, FH-	AD vs APOE4 +, FH +	Control vs APOE4-, FH-	Control vs APOE4 +, FH +	APOE4-, FH- vs APOE4 +, FH +
LF flow range ICA	0.005*	0.010*	< 0.001*	0.999	0.537	0.516
C flow range ICA	0.863	0.920	0.551	0.403	0.906	0.173
LF flow range SSS	0.492	0.191	0.005*	0.888	0.090	0.365
C flow range SSS	0.458	0.999	0.459	0.478	0.999	0.483
Std flow ICA	0.011*	0.043*	< 0.001*	0.980	0.316	0.188
Std/(ICV-CSF) flow ICA	0.040*	0.471	0.044*	0.601	0.995	0.541
Std flow SSS	0.536	0.439	0.003*	0.996	0.057	0.115
Std/(ICV-CSF) flow SSS	0.789	0.865	0.070	0.999	0.279	0.255
Avg flow ICA	0.071	0.004*	< 0.001*	0.637	0.022*	0.322
Avg flow SSS	0.780	0.120	0.006*	0.449	0.034*	0.545

Control refers to the age-matched control group (age-matched to AD group). *Statistically Significant (P < 0.05). Abbreviations: AD, Alzheimer's disease; APOE, apolipoprotein E; Avg, average; C, cardiac (from cardiac reconstruction); CSF, cerebrospinal fluid; FH, family history; ICV, intracranial volume; LF, low frequency (from time reconstruction); SSS, superior sagittal sinus; Std, standard deviation.

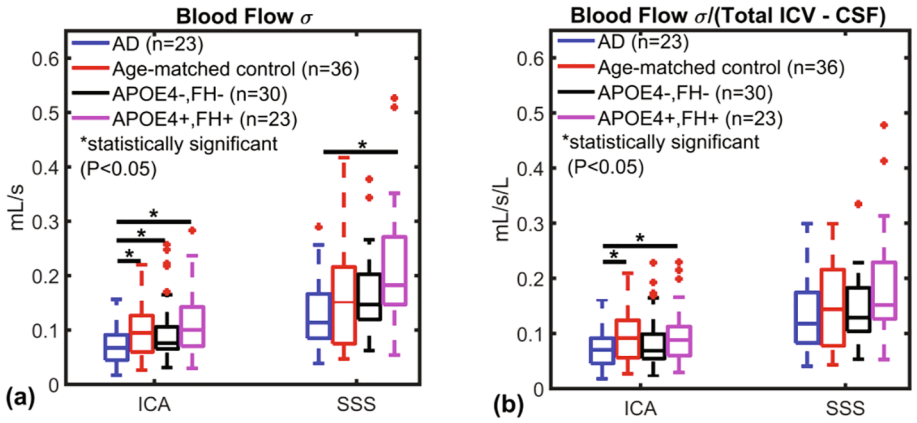

Fig. 5. Box plots showing the standard deviations of the flow time series (a), and brain volume (total ICV-CSF) normalized standard deviations (b) in Alzheimer's' disease (AD) subjects (n = 23), age-matched control subjects (n = 36), late middle-aged APOE4-, FH- subjects (n = 30), and late middle-aged APOE4 +, FH + subjects (n = 23). Lowest standard deviations were measured in AD subjects.

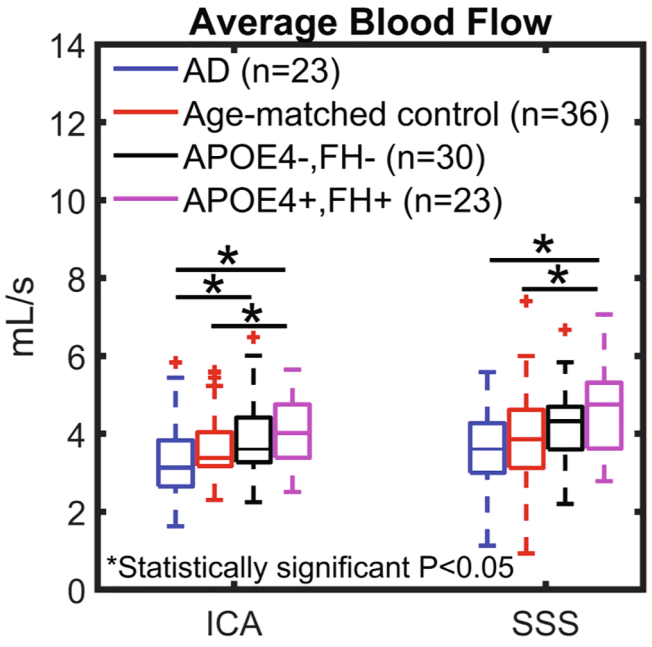

Fig. 6. Box plots showing average blood flow derived from time-resolved data in Alzheimer's disease (AD) subjects (n = 23), age-matched control subjects (n = 36), late middle-aged APOE4-, FH- subjects (n = 30), and late middle-aged APOE4 +, FH + subjects (n = 23). Blood flow was lowest in AD subjects, followed by age-matched control subjects, late middle-aged APOE4-, FH- subjects, and late middle-aged APOE4 +, FH + subjects.

finally to veins. In a healthy system, arterial compliance reduces cardiac pulsations as they travel along the arterial tree. Cardiac pulsations are further dampened in the brain inducing tissue strain changes (Adams et al., 2019). By the time the cardiac pulse wave reaches the venous return its pulsatility has been reduced substantially which is observed in the lower SSS high frequency cardiac flow range measurements. Previous measures of arterial and venous pulsatility in the intracranial arteries and veins also showed lower pulsatility in veins (Rivera-Rivera et al., 2017). Compared to high frequency cardiac pulsations, LFOs flow range in the arteries is related to auto regulatory mechanisms and cerebrovascular vasomotion from contraction and relaxation of smooth muscle cells. The venous wall is thinner than the arterial wall with less smooth muscle and connective tissue. Given this, venous LFOs are likely less related to auto regulation and vasomotion and driven by other factors such as breathing, upstream arterial and capillary changes, and thoracic pressure changes which might explain the larger venous LFO flow range observed in this study.

PSD analysis showed LFOs were smallest in AD subjects followed by age-matched controls, late middle-aged APOE4-, FH-, and APOE4 +, FH +. The standard deviations of the arterial time series were significantly smaller in AD when compared with other groups. After normalizing to brain volumes, significantly lower standard deviations in the ICA time series were measured between AD subjects and age-matched controls. These correlations were not as strong in the venous segment (SSS); however, in this study, velocity sensitivity was optimized for arteries at the expense of decreased sensitivity to the lower velocities found in veins. CHS scores from T2FLAIR images where used to quantify WMH burden. CHS scores allow radiologists take into consideration subject age and WMH longitudinal progression during scoring. In this study, CHS scores showed higher degree of WMH in AD patients compared to controls; however, differences were not significant. These findings suggests small vessel disease, with WMH used as a representative vascular marker, might contribute to LFOs measurements; however, LFO differences between AD and controls were significant, suggesting additional contributions besides those of small vessel disease burden origin. Blood flow rates from time-resolved 4D flow were lower in AD, followed by age-matched controls, late middle-aged APOE4-, FH-, and APOE4 +, FH +, agreeing with previous studies on AD groups and subjects at risk for AD (Clark et al., 2017; Rivera-Rivera et al., 2016; Roher et al., 2011); however, similar to WMH, blood flow rates might not specifically characterize the vasculature but can be driven by neuron metabolism, for example.

Further work is needed to more fully evaluate and optimize the LFOs measures from 4D flow MRI. In this work, comparison in phantoms and breath holds in subjects were the primary methods used for evaluation. Phantom experiments demonstrated good agreement between 4D and 2D techniques; however, 4D showed larger measurement variance. The larger variance in 4D data was observed in all phantom experiments, including in the flow compensated acquisition. This result is not surprising since the 4D data were heavily undersampled compared to fully sampled 2D scans. Magnitude images from the time series (supplementary Fig. 1) showed inflow effects and intravoxel dephasing in both type of acquisitions, but larger effects were seen on 4D data. Volunteer BH experiments were performed to assess the capacity of 4D flow imaging to measure physiological changes during a mild challenge. During the BH, flow decreased in the SSS, and similar responses were measured using 4D and 2D methods; however, the physiological response in 2D images was larger, suggesting higher sensitivity of the 2D approach under physiological conditions. The higher V_{enc} of the 4D flow scan (100 vs 80 cm/s) could have also contributed to decreased sensitivity of the 4D technique to venous flow. Interestingly, standard deviations were also larger in 2D than in 4D measures. Respiratory variability between scans likely contribute to standard deviation differences. For example, subject #4 2D scan measurements show larger standard deviations; by inspecting the respiratory bellows data (supplementary Fig. 2), this subject shows more variability in the respiratory pattern during the 2D scan compared to the 4D scan. The observed flow drop in the SSS during the BH task in both 2D and 4D

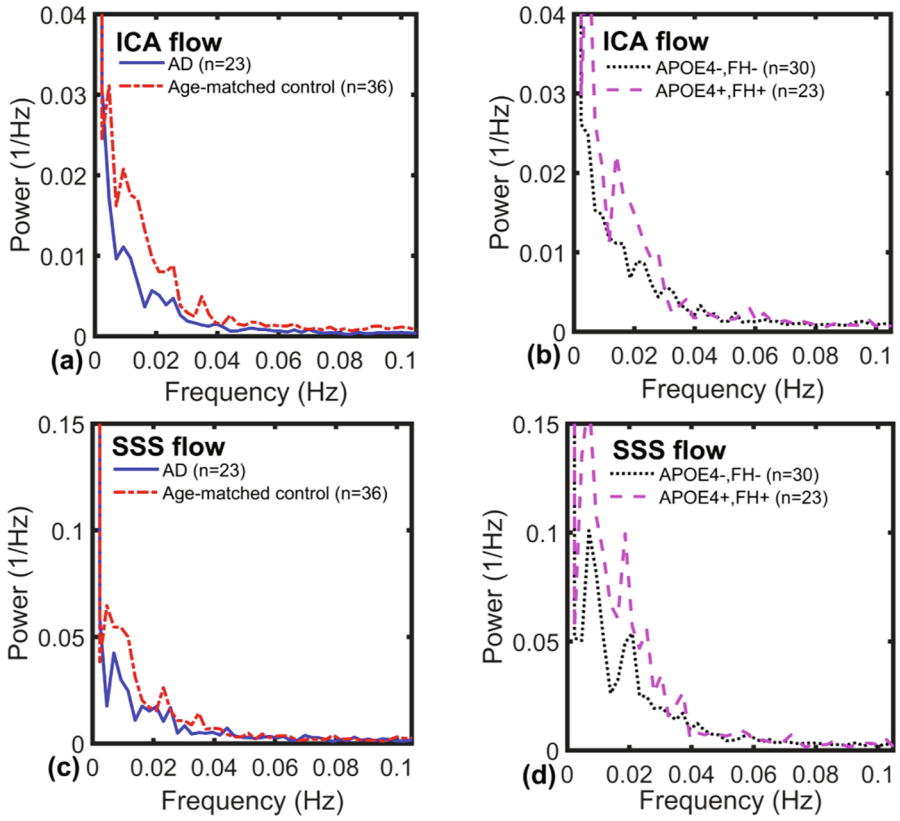

Fig. 7. Power spectrum density (PSD) plots showing average low frequency content derived from time-resolved flow data in the internal carotid artery (ICA) (a, b) and superior sagittal sinus (SSS) (c, d) of Alzheimer's' disease (AD) subjects (n = 23) (a, c), age-matched control subjects (n = 36) (a, c), late middle-aged APOE4-, FH- subjects (n = 30) (b, d), and late middle-aged APOE4+, FH + subjects (n = 23) (b, d). Diminished frequency content was measured in AD when compared with age-matched controls. Late middle-age APOE4+, FH + subjects showed largest flow low frequency oscillations.

measures likely means the BH task was too mild to induce significant CO2 changes. Furthermore, it is possible participants inadvertently did a valsalva maneuver instead which leads to the sudden creation and maintenance of a positive intrathoracic pressure (Kudo et al., 2004; Mehta et al., 2000). The creation of a positive intrathoracic pressure can result from full inspiration, followed by closing of the glottis and can lead to decreased intracranial venous return from the sinuses. The arterial signals during the volunteer BH experiments were challenge by accurate 2D plane placement orthogonally to the ICA and motion sensitivity during the BH task on the 2D scan, leading to large variability, for this reason arterial signals were excluded from the volunteer BH experiments. Further work is needed to compare 4D flow signals during BH tasks and more challenging tasks such as hypercapnia with local flow fluctuations from rs-fMRI and from NIRS, both of which were not available in this study.

This study has several limitations. Material and arterial/vein compliance matching was not considered in the physical model experiments limiting technique validation. The 4D flow MRI sequence in subject's population is part of a larger imaging protocol that was originally optimized for high spatial and low temporal resolution imaging. Therefore, in this study, spatial resolution was traded during the reconstruction for higher temporal binning leading to a spatial resolution of 1.38 mm isotropic. The lower spatial resolution limits the analysis to relatively large arteries such as the ICA, while LFO measures in smaller arteries closer to the brain tissue such as the middle cerebral artery (MCA) would be of interest. A small artery optimized protocol could be designed to address this limitation. Methods to correct for bulk motion are needed to improve time-resolved imaging reproducibility and robustness. In this study, images were inspected visually for bulk motion (supplementary Fig. 3), but motion correction methods should be employed to minimize data loss and confounding effects. BOLD fMRI studies (Birn et al., 2006) have shown variations in respiration depth from breath to breath can affect fMRI signal and the frequency of these respiratory changes (~0.03 Hz) overlaps with the frequencies of fluctuations from varying brain activity at rest (< 0.1 Hz). In our study we did not explore potential effects from breath to breath variations to 4D flow based LFO measurements. Unfortunately, respiratory bellows data were not available for AD studies. It should be noted 4D flow measurements are based on phase contrast signal changes, while BOLD measurements from R2* signal changes and the latter is more sensitive to venous drainage variability due the changes in intrathoracic pressure and respiratory induced susceptibility changes which can add bias to center frequencies measured during the fMRI experiment. Further, it cannot be entirely ruled out that the observed deficits in LFOs in clinical AD subjects are partially driven by impairment in vascular tone attributed to concomitant cerebral small vessel disease and WMH that damages sympathetic adrenergic nerves found in the adventitia. Amyloid and tau pathology from AD biomarker confirmed subjects needs to be correlated with LFOs in order to establish the type of relationship between AD and LFOs. Transcranial PWV was significantly higher in AD subjects compared to controls suggesting arterial stiffness and vascular remodeling in AD subjects; however, linear correlation between transcranial PWV with LFO markers was weak suggesting other factors might contribute to the observed LFO differences between AD and age-matched controls. In this study we tried to measure delayed transit times from ICA to SSS using LFO measurements from 4D flow MRI, similar to what other researchers (Tong et al., 2019b) performed using systemic LFO measurements from BOLD signals. They measured delayed transit times from ICA to SSS on the order of 6.07 sec. Unfortunately, temporal resolution in our study was insufficient to distinguish the curves delay. In the researchers experiment fMRI scans where acquired at a temporal resolution of 1.16 sec, while in our study temporal resolution was 4.30 sec. In addition, the researchers use data from a 45 year old healthy subject, while here we study an older population (mean age 66yrs) including clinical AD subjects for which LFOs time delays could be different. Also, the BOLD signal and flow changes likely don't measure the same effect, with the BOLD signal being inherently coupled to oxygenation changes and bulk transport.

Future 4D flow MRI LFO studies should explore higher temporal resolution if possible.

5. Conclusions

High frame rate, time-resolved 4D flow MRI based spontaneous LFO measures are feasible and significantly reduced in clinically diagnosed AD subjects when compared to age-matched controls. The effects of vascular modifications on the neuropathologic trajectory of AD remains poorly understood. Future studies should investigate the relation between LFOs markers and AD biomarkers, including amyloid and tau pathology. LFO measurements hold potential for longitudinal studies aiming at predicting cognitive trajectories and understanding the relationship between AD and CVD.

Funding

This work was supported by the Alzheimer's Association [grant number AARFD-20-678095]; and the National Institutes of Health [grant numbers R01NS066982, P50-AG033514, R01AG021155, and R01EB027087].

7. Data availability

Data from the core WRAP protocol study in partnership with the WADRC are accessible to qualified researchers via an online request form and data use agreement which can be linked from the Global Alzheimer's Association Interactive Network web site (www.gaain.org). Prior to data access, users are required to agree to the data use agreement – essential for data security, grant citation, and annual progress reports.

Disclosure/Conflict of interest

S.C. Johnson served on an advisory board for Roche Diagnostics in 2018 for which he received an honorarium and is principal investigator of an equipment grant from Roche. He conducts tau imaging in NIH funded studies as well as a study funded by Cerveau Technologies using radioligand precursor material supplied by Cerveau Technologies.

CRediT authorship contribution statement

Leonardo A. Rivera-Rivera: Conceptualization, Formal analysis, Funding acquisition, Investigation, Methodology, Software, Visualization, Writing - original draft. **Karly A. Cody:** Data curation, Resources. **David Rutkowski:** Methodology, Resources, Writing - review & editing. **Paul Cary:** Data curation, Resources. **Laura Eisenmenger:** Resources, Supervision, Writing - review & editing. **Howard A. Rowley:** Resources, Supervision. **Cynthia M. Carlsson:** Resources, Supervision. **Sterling C. Johnson:** Funding acquisition, Investigation, Supervision, Resources, Supervision, Writing - review & editing. **Kevin M. Johnson:** Conceptualization, Funding acquisition, Investigation, Methodology, Supervision, Software, Writing - review & editing.

Acknowledgement

We gratefully acknowledge research support from GE Healthcare, Waukesha, WI , USA..

Appendix A. Supplementary data

Supplementary data to this article can be found online at https://doi.org/10.1016/j.nicl.2020.102379.

References

Adams, A.L., Viergever, M.A., Luijten, P.R., Zwanenburg, J.J.M., 2020. Validating faster DENSE measurements of cardiac-induced brain tissue expansion as a potential tool for investigating cerebral microvascular pulsations. NeuroImage 208, 116466. https://doi.org/10.1016/j.neuroimage.2019.116466.

Alber, J., Alladi, S., Bae, H.-J., Barton, D.A., Beckett, L.A., Bell, J.M., Berman, S.E., Biessels, G.J., Black, S.E., Bos, I., Bowman, G.L., Brai, E., Brickman, A.M., Callahan, B.L., Corriveau, R.A., Fossati, S., Gottesman, R.F., Gustafson, D.R., Hachinski, V., Hayden, K.M., Helman, A.M., Hughes, T.M., Isaacs, J.D., Jefferson, A.L., Johnson, S.C., Kapasi, A., Kern, S., Kwon, J.C., Kukolja, J., Lee, A., Lockhart, S.N., Murray, A., Osborn, K.E., Power, M.C., Price, B.R., Rhodius-Meester, H.F.M., Rondeau, J.A., Rosen, A.C., Rosene, D.L., Schneider, J.A., Scholtzova, H., Shaaban, C.E., Silva, N.C.B.S., Snyder, H.M., Swardfager, W., Troen, A.M., Veluw, S.J., Vemuri, P., Wallin, A., Wellington, C., Wilcock, D.M., Xie, S.X., Hainsworth, A.H., 2019. White matter hyperintensities in vascular contributions to cognitive impairment and dementia (VCID): Knowledge gaps and opportunities. Alzheimer's Dementia: Transl. Res. Clin. Intervent. 5 (1), 107–117.

Albert, M.S., DeKosky, S.T., Dickson, D., Dubois, B., Feldman, H.H., Fox, N.C., Gamst, A., Holtzman, D.M., Jagust, W.J., Petersen, R.C., Snyder, P.J., Carrillo, M.C., Thies, B., Phelps, C.H., 2011. The diagnosis of mild cognitive impairment due to Alzheimer's disease: recommendations from the National Institute on Aging-Alzheimer's Association workgroups on diagnostic guidelines for Alzheimer's disease. Alzheimer's Dementia 7 (3), 270–279.

Aldea, R., Weller, R.O., Wilcock, D.M., Carare, R.O., Richardson, G., 2019. Cerebrovascular smooth muscle cells as the drivers of intramural periarterial drainage of the brain. Front. Aging Neurosci. 11. https://doi.org/10.3389/fnagi.2019.00001.

Allison, S.L., Koscik, R.L., Cary, R.P., Jonaitis, E.M., Rowley, H.A., Chin, N.A., Zetterberg, H., Blennow, K., Carlsson, C.M., Asthana, S., Bendlin, B.B., Johnson, S.C., 2019. Comparison of different MRI-based morphometric estimates for defining neurodegeneration across the Alzheimer's disease continuum. NeuroImage: Clin. 23, 101895. https://doi.org/10.1016/j.nicl.2019.101895.

Andersen, A.V., Simonsen, S.A., Schytz, H.W., Iversen, H.K., 2018. Assessing low-frequency oscillations in cerebrovascular diseases and related conditions with near-infrared spectroscopy: a plausible method for evaluating cerebral autoregulation? Neurophotonics 5 (03), 1. https://doi.org/10.1117/1.NPh.5.3.030901.

Arvanitakis, Z., Capuano, A.W., Leurgans, S.E., Bennett, D.A., Schneider, J.A., 2016. Relation of cerebral vessel disease to Alzheimer's disease dementia and cognitive function in elderly people: a cross-sectional study. Lancet Neurol. 15 (9), 934–943.

Berman, S.E., Clark, L.R., Rivera-Rivera, L.A., Norton, D., Racine, A.M., Rowley, H.A., Bendlin, B.B., Blennow, K., Zetterberg, H., Carlsson, C.M., Asthana, S., Turski, P., Wieben, O., Johnson, S.C., Naranjo, I.C., 2017. Intracranial arterial 4D flow in individuals with mild cognitive impairment is associated with cognitive performance and amyloid positivity. JAD 60 (1), 243–252.

Berman, S.E., Rivera-Rivera, L.A., Clark, L.R., Racine, A.M., Keevil, J.G., Bratzke, L.C., Carlsson, C.M., Bendlin, B.B., Rowley, H.A., Blennow, K., Zetterberg, H., Asthana, S., Turski, P., Johnson, S.C., Wieben, O., 2015. Intracranial arterial four-dimensional flow is associated with metrics of brain health and Alzheimer's disease. Alzheimer's Dementia: Diagn. Assessment Disease Monitor. 1 (4), 420–428.

Birdsill, A.C., Koscik, R.L., Jonaitis, E.M., Johnson, S.C., Okonkwo, O.C., Hermann, B.P., LaRue, A., Sager, M.A., Bendlin, B.B., 2014. Regional white matter hyperintensities: aging, Alzheimer's disease risk, and cognitive function. Neurobiol. Aging 35 (4), 769–776.

Birn, R.M., Diamond, J.B., Smith, M.A., Bandettini, P.A., 2006. Separating respiratory-variation-related fluctuations from neuronal-activity-related fluctuations in fMRI. NeuroImage 31 (4), 1536–1548.

Carare, R.O., Aldea, R., Bulters, D., Alzetani, A., Birch, A.A., Richardson, G., Weller, R.O., 2020. Vasomotion drives periarterial drainage of aβ from the brain. Neuron 105 (3), 400–401.

Chow, B.W., Nuñez, V., Kaplan, L., Granger, A.J., Bistrong, K., Zucker, H.L., Kumar, P., Sabatini, B.L., Gu, C., 2020. Caveolae in CNS arterioles mediate neurovascular coupling. Nature 579 (7797), 106–110.

Clark, L.R., Berman, S.E., Rivera-Rivera, L.A., Hoscheidt, S.M., Darst, B.F., Engelman, C.D., Rowley, H.A., Carlsson, C.M., Asthana, S., Turski, P., Wieben, O., Johnson, S.C., 2017. Macrovascular and microvascular cerebral blood flow in adults at risk for Alzheimer's disease. Alzheimer's Dementia: Diagn. Assessment Disease Monitor. 7 (1), 48–55.

Dementia: Fact sheet N°362. World Health Organization (WHO) 2019 [cited 2019 September]. Available from: [WWW Document], n.d. URL https://www.who.int/en/news-room/fact-sheets/detail/dementia.

Di Marco, L.Y., Farkas, E., Martin, C., Venneri, A., Frangi, A.F., 2015. Is vasomotion in cerebral arteries impaired in Alzheimer's disease? JAD 46 (1), 35–53.

Diem, A.K., MacGregor Sharp, M., Gatherer, M., Bressloff, N.W., Carare, R.O., Richardson, G., 2017. Arterial pulsations cannot drive intramural periarterial drainage: significance for aβ drainage. Front. Neurosci. 11, 475. https://doi.org/10.3389/fnins.2017.00475.

Hawkes, C.A., Jayakody, N., Johnston, D.A., Bechmann, I., Carare, R.O., 2014. Failure of perivascular drainage of β-amyloid in cerebral amyloid angiopathy: failure of perivascular drainage of β-amyloid. Brain Pathol. 24 (4), 396–403.

Hussein, A., Matthews, J.L., Syme, C., Macgowan, C., MacIntosh, B.J., Shirzadi, Z., Pausova, Z., Paus, T., Chen, J.J., 2020. The association between resting-state functional magnetic resonance imaging and aortic pulse-wave velocity in healthy adults. Hum. Brain Mapp. 41 (8), 2121–2135.

Iliff, J.J., Wang, M., Liao, Y., Plogg, B.A., Peng, W., Gundersen, G.A., Benveniste, H., Vates, G.E., Deane, R., Goldman, S.A., Nagelhus, E.A., Nedergaard, M., 2012. A paravascular pathway facilitates CSF flow through the brain parenchyma and the clearance of interstitial solutes, including amyloid. Sci. Transl. Med. 4 (147), 147ra111.

Jack Jr., C.R., Bennett, D.A., Blennow, K., Carrillo, M.C., Dunn, B., Haeberlein, S.B.,

Holtzman, D.M., Jagust, W., Jessen, F., Karlawish, J., Liu, E., Molinuevo, J.L., Montine, T., Phelps, C., Rankin, K.P., Rowe, C.C., Scheltens, P., Siemers, E., Snyder, H.M., Sperling, R., Elliott, C., Masliah, E., Ryan, L., Silverberg, N., 2018. NIA-AA research framework: toward a biological definition of Alzheimer's disease. Alzheimer's Dementia 14 (4), 535–562.

Jessen, N.A., Munk, A.S.F., Lundgaard, I., Nedergaard, M., 2015. The glymphatic system: a beginner's guide. Neurochem. Res. 40 (12), 2583–2599.

Jimenez, J.E., Strigel, R.M., Johnson, K.M., Henze Bancroft, L.C., Reeder, S.B., Block, W.F., 2018. Feasibility of high spatiotemporal resolution for an abbreviated 3D radial breast MRI protocol. Magn. Reson. Med. 80 (4), 1452–1466.

Johnson, K.M., Lum, D.P., Turski, P.A., Block, W.F., Mistretta, C.A., Wieben, O., 2008. Improved 3D phase contrast MRI with off-resonance corrected dual echo VIPR: improved 3D PC MRI With corrected dual echo VIPR. Magn. Reson. Med. 60 (6), 1329–1336.

Johnson, S.C., Koscik, R.L., Jonaitis, E.M., Clark, L.R., Mueller, K.D., Berman, S.E., Bendlin, B.B., Engelman, C.D., Okonkwo, O.C., Hogan, K.J., Asthana, S., Carlsson, C.M., Hermann, B.P., Sager, M.A., 2018. The Wisconsin registry for Alzheimer's prevention: a review of findings and current directions. Alzheimer's Dementia: Diagn. Assessment Disease Monitor. 10 (1), 130–142.

Kudo, K., Terae, S., Ishii, A., Omatsu, T., Asano, T., Tha, K., Miyasaka, K., 2004. Physiologic change in flow velocity and direction of dural venous sinuses with respiration: MR venography and flow analysis. Am. J. Neuroradiol. 25, 551.

Laurent, S., Cockcroft, J., Van Bortel, L., Boutouyrie, P., Giannattasio, C., Hayoz, D., Pannier, B., Vlachopoulos, C., Wilkinson, I., Struijker-Boudier, H., on behalf of the European Network for Non-invasive Investigation of Large Arteries, 2006. Expert consensus document on arterial stiffness: methodological issues and clinical applications. Eur. Heart J. 27, 2588–2605. https://doi.org/10.1093/eurheartj/ehl254.

Manolio, T.A., Kronmal, R.A., Burke, G.L., Poirier, V., O'Leary, D.H., Gardin, J.M., Fried, L.P., Steinberg, E.P., Bryan, R.N., 1994. Magnetic resonance abnormalities and cardiovascular disease in older adults. The cardiovascular health study. Stroke 25 (2), 318–327.

McKhann, G., Drachman, D., Folstein, M., Katzman, R., Price, D., Stadlan, E.M., 1984. Clinical diagnosis of Alzheimer's disease: report of the NINCDS-ADRDA Work Group* under the auspices of Department of Health and Human Services Task Force on Alzheimer's Disease. Neurology 34 (7), 939–944.

McKhann, G.M., Knopman, D.S., Chertkow, H., Hyman, B.T., Jack Jr., C.R., Kawas, C.H., Klunk, W.E., Koroshetz, W.J., Manly, J.J., Mayeux, R., Mohs, R.C., Morris, J.C., Rossor, M.N., Scheltens, P., Carrillo, M.C., Thies, B., Weintraub, S., Phelps, C.H., 2011. The diagnosis of dementia due to Alzheimer's disease: recommendations from the National Institute on Aging-Alzheimer's Association workgroups on diagnostic guidelines for Alzheimer's disease. Alzheimer's Dementia 7 (3), 263–269.

Mehta, N.R., Jones, L., Kraut, M.A., Melhem, E.R., 2000. Physiologic variations in dural venous sinus flow on phase-contrast MR imaging. Am. J. Roentgenol. 175 (1), 221–225.

Mestre, H., Tithof, J., Du, T., Song, W., Peng, W., Sweeney, A.M., Olveda, G., Thomas, J.H., Nedergaard, M., Kelley, D.H., 2018. Flow of cerebrospinal fluid is driven by arterial pulsations and is reduced in hypertension. Nat. Commun. 9 (1). https://doi.org/10.1038/s41467-018-07318-3.

Moghekar, A., Kraut, M., Elkins, W., Troncoso, J., Zonderman, A.B., Resnick, S.M., O'Brien, R.J., 2012. Cerebral white matter disease is associated with Alzheimer pathology in a prospective cohort. Alzheimer's Dementia 8, S71–S77.

Obrig, H., Neufang, M., Wenzel, R., Kohl, M., Steinbrink, J., Einhäupl, K., Villringer, A., 2000. Spontaneous low frequency oscillations of cerebral hemodynamics and metabolism in human adults. NeuroImage 12 (6), 623–639.

Ong, F., Lustig, M., n.d. SigPy: A python package for high performance iterative reconstruction. In: 27th Annual ISMRM Meeting, Montreal, Canada, p. 4819.

Plog, B.A., Nedergaard, M., 2018. The glymphatic system in central nervous system health and disease: past, present, and future. Annu. Rev. Pathol. Mech. Dis. 13 (1), 379–394.

Pruessmann, K.P., Weiger, M., Scheidegger, M.B., Boesiger, P., 1999. SENSE: sensitivity encoding for fast MRI. Magn. Reson. Med. 42 (5), 952–962.

Quaresima, V., Ferrari, M., 2019. Functional near-infrared spectroscopy (fNIRS) for assessing cerebral cortex function during human behavior in natural/social situations: a concise review. Organ. Res. Methods 22 (1), 46–68.

Rivera-Rivera, L.A., Cody, K.A., Eisenmenger, L., Cary, P., Rowley, H.A., Carlsson, C.M., Johnson, S.C., Johnson, K.M., 2020. Assessment of vascular stiffness in the internal carotid artery proximal to the carotid canal in Alzheimer's disease using pulse wave velocity from low rank reconstructed 4D flow MRI. J. Cereb. Blood. Flow Metab. 0271678X20910302. https://doi.org/10.1177/0271678X20910302.

Rivera-Rivera, L.A., Schubert, T., Turski, P., Johnson, K.M., Berman, S.E., Rowley, H.A., Carlsson, C.M., Johnson, S.C., Wieben, O., 2017. Changes in intracranial venous blood flow and pulsatility in Alzheimer's disease: a 4D flow MRI study. J. Cereb. Blood Flow Metab. 37 (6), 2149–2158.

Rivera-Rivera, L.A., Turski, P., Johnson, K.M., Hoffman, C., Berman, S.E., Kilgas, P., Rowley, H.A., Carlsson, C.M., Johnson, S.C., Wieben, O., 2016. 4D flow MRI for intracranial hemodynamics assessment in Alzheimer's disease. J. Cereb. Blood Flow Metab. 36 (10), 1718–1730.

Roher, A.E., Garami, Z., Tyas, S.L., Maarouf, C.L., Kokjohn, T.A., Belohlavek, M., Vedders, L.J., Connor, D., Sabbagh, M.N., Beach, T.G., Emmerling, M.R., 2011. Transcranial Doppler ultrasound blood flow velocity and pulsatility index as systemic indicators for Alzheimer's disease. Alzheimer's Dementia 7 (4), 445–455.

Schrauben, E., Wåhlin, A., Ambarki, K., Spaak, E., Malm, J., Wieben, O., Eklund, A., 2015. Fast 4D flow MRI intracranial segmentation and quantification in tortuous arteries: fast 4D flow processing tool. J. Magn. Reson. Imaging 42 (5), 1458–1464.

Sperling, R.A., Aisen, P.S., Beckett, L.A., Bennett, D.A., Craft, S., Fagan, A.M., Iwatsubo, T., Jack Jr., C.R., Kaye, J., Montine, T.J., Park, D.C., Reiman, E.M., Rowe, C.C., Siemers, E., Stern, Y., Yaffe, K., Carrillo, M.C., Thies, B., Morrison-Bogorad, M., Wagster, M.V., Phelps, C.H., 2011. Toward defining the preclinical stages of Alzheimer's disease: recommendations from the National Institute on Aging-Alzheimer's Association workgroups on diagnostic guidelines for Alzheimer's disease. Alzheimer's Dementia 7 (3), 280–292.

Summers, P.E., Holdsworth, D.W., Nikolov, H.N., Rutt, B.K., Drangova, M., 2005. Multisite trial of MR flow measurement: phantom and protocol design. J. Magn. Reson. Imaging 21 (5), 620–631.

Sweeney, M.D., Montagne, A., Sagare, A.P., Nation, D.A., Schneider, L.S., Chui, H.C., Harrington, M.G., Pa, J., Law, M., Wang, D.J.J., Jacobs, R.E., Doubal, F.N., Ramirez, J., Black, S.E., Nedergaard, M., Benveniste, H., Dichgans, M., Iadecola, C., Love, S., Bath, P.M., Markus, H.S., Salman, R.A., Allan, S.M., Quinn, T.J., Kalaria, R.N., Werring, D.J., Carare, R.O., Touyz, R.M., Williams, S.C.R., Moskowitz, M.A., Katusic, Z.S., Lutz, S.E., Lazarov, O., Minshall, R.D., Rehman, J., Davis, T.P., Wellington, C.L., González, H.M., Yuan, C., Lockhart, S.N., Hughes, T.M., Chen, C.L.H., Sachdev, P., O'Brien, J.T., Skoog, I., Pantoni, L., Gustafson, D.R., Biessels, G.J., Wallin, A., Smith, E.E., Mok, V., Wong, A., Passmore, P., Barkof, F., Muller, M., Breteler, M.M.B., Román, G.C., Hamel, E., Seshadri, S., Gottesman, R.F., van Buchem, M.A., Arvanitakis, Z., Schneider, J.A., Drewes, L.R., Hachinski, V., Finch, C.E., Toga, A.W., Wardlaw, J.M., Zlokovic, B.V., 2019. Vascular dysfunction-the disregarded partner of Alzheimer's disease. Alzheimer's Dementia 15 (1), 158–167.

Sweeney, M.D., Sagare, A.P., Zlokovic, B.V., 2018. Blood–brain barrier breakdown in Alzheimer disease and other neurodegenerative disorders. Nat. Rev. Neurol. 14 (3), 133–150.

Sweeney, M.D., Sagare, A.P., Zlokovic, B.V., 2015. Cerebrospinal fluid biomarkers of neurovascular dysfunction in mild dementia and Alzheimer's disease. J. Cereb. Blood Flow Metab. 35 (7), 1055–1068.

The SPRINT MIND Investigators for the SPRINT Research Group, 2019. Effect of intensive vs standard blood pressure control on probable dementia: a randomized clinical trial. JAMA 321, 553–561. https://doi.org/10.1001/jama.2018.21442.

Toledo, J.B., Arnold, S.E., Raible, K., Brettschneider, J., Xie, S.X., Grossman, M., Monsell, S.E., Kukull, W.A., Trojanowski, J.Q., 2013. Contribution of cerebrovascular disease in autopsy confirmed neurodegenerative disease cases in the National Alzheimer's Coordinating Centre. Brain 136, 2697–2706. https://doi.org/10.1093/brain/awt188.

Tong, Y., Frederick, B., 2010. Time lag dependent multimodal processing of concurrent fMRI and near-infrared spectroscopy (NIRS) data suggests a global circulatory origin for low-frequency oscillation signals in human brain. NeuroImage 53 (2), 553–564.

Tong, Y., Hocke, L.M., Frederick, B.B., 2019a. Low frequency systemic hemodynamic "Noise" in resting state BOLD fMRI: characteristics, causes, implications, mitigation strategies, and applications. Front. Neurosci. 13, 787. https://doi.org/10.3389/fnins.2019.00787.

Tong, Y., Hocke, L.M., Licata, S.C., Frederick, B.d., 2012. Low-frequency oscillations measured in the periphery with near-infrared spectroscopy are strongly correlated with blood oxygen level-dependent functional magnetic resonance imaging signals. J. Biomed. Opt. 17 (10), 1. https://doi.org/10.1117/1.JBO.17.10.10600410.1117/1.JBO.17.10.106004.1.

Tong, Y., Hocke, L.M., Lindsey, K.P., Erdoğan, S.B., Vitaliano, G., Caine, C.E., Frederick, B. de B., 2016. Systemic low-frequency oscillations in BOLD signal vary with tissue type. Front. Neurosci. 10. https://doi.org/10.3389/fnins.2016.00313.

Tong, Yunjie, Yao, Jinxia (Fiona), Chen, J Jean, Frederick, Blaise de B., 2019b. The resting-state fMRI arterial signal predicts differential blood transit time through the brain. J. Cereb. Blood Flow Metab. 39 (6), 1148–1160.

Trzasko, J.D., Manduca, A., 2011. Calibrationless parallel MRI using CLEAR, in: 2011 Conference Record of the Forty Fifth Asilomar Conference on Signals, Systems and Computers (ASILOMAR). In: Presented at the 2011 45th Asilomar Conference on Signals, Systems and Computers, IEEE, Pacific Grove, CA, USA, pp. 75–79. https://doi.org/10.1109/ACSSC.2011.6189958.

van Veluw, Susanne J., Hou, Steven S., Calvo-Rodriguez, Maria, Arbel-Ornath, Michal, Snyder, Austin C., Frosch, Matthew P., Greenberg, Steven M., Bacskai, Brian J., 2020. Vasomotion as a driving force for paravascular clearance in the awake mouse brain. Neuron 105 (3), 549–561.e5.

Vikner, T., Nyberg, L., Holmgren, M., Malm, J., Eklund, A., Wåhlin, A., 2019. Characterizing pulsatility in distal cerebral arteries using 4D flow MRI. J Cereb Blood Flow Metab 0271678X19886667. https://doi.org/10.1177/0271678X19886667.

Wåhlin, Anders, Nyberg, Lars, 2019. At the heart of cognitive functioning in aging. Trends Cogn. Sci. 23 (9), 717–720.

Wardlaw, J.M., Smith, E.E., Biessels, G.J., Cordonnier, C., Fazekas, F., Frayne, R., Lindley, R.I., O'Brien, J.T., Barkhof, F., Benavente, O.R., Black, S.E., Brayne, C., Breteler, M., Chabriat, H., Decarli, C., de Leeuw, F.-E., Doubal, F., Duering, M., Fox, N.C., Greenberg, S., Hachinski, V., Kilimann, I., Mok, V., van Oostenbrugge, R., Pantoni, L., Speck, O., Stephan, B.C.M., Teipel, S., Viswanathan, A., Werring, D., Chen, C., Smith, C., van Buchem, M., Norrving, B., Gorelick, P.B., Dichgans, M., STandards for ReportIng Vascular changes on nEuroimaging (STRIVE v1), 2013. Neuroimaging standards for research into small vessel disease and its contribution to ageing and neurodegeneration. Lancet Neurol. 12, 822–838. https://doi.org/10.1016/S1474-4422(13)70124-8.

Weller, R.O., Boche, D., Nicoll, J.A.R., 2009. Microvasculature changes and cerebral amyloid angiopathy in Alzheimer's disease and their potential impact on therapy. Acta Neuropathol. 118, 87–102. https://doi.org/10.1007/s00401-009-0498-z.

Ying, Leslie, Sheng, Jinhua, 2007. Joint image reconstruction and sensitivity estimation in SENSE (JSENSE). Magn. Reson. Med. 57 (6), 1196–1202.

Zeller, Julia B.M., Katzorke, Andrea, Müller, Laura D., Breunig, Judith, Haeussinger, Florian B., Deckert, Jürgen, Warrings, Bodo, Lauer, Martin, Polak, Thomas, Herrmann, Martin J., 2019. Reduced spontaneous low frequency oscillations as measured with functional near-infrared spectroscopy in mild cognitive impairment. Brain Imag. Behav. 13 (1), 283–292.